Phase synchronization of three locally coupled chaotic electrochemical oscillators: Enhanced phase diffusion and identification of indirect coupling

Mahesh Wickramasinghe and István Z. Kiss*

Saint Louis University, Department of Chemistry, 3501 Laclede Avenue, St. Louis, Missouri 63103, USA

(Received 25 September 2010; revised manuscript received 22 November 2010; published 21 January 2011)

Experiments are carried out with three locally coupled phase coherent chaotic electrochemical oscillators (*A*-*B*-*C*) in nickel dissolution in sulfuric acid. As the interaction strength is increased among the electrodes, an onset of synchronization is observed where the frequencies become identical and the phase differences are bounded. The precision of the period of the oscillators is characterized by phase diffusion coefficients from phases and phase differences. The transition to synchronization with increase of coupling strength was found to be accompanied by enhanced phase fluctuations that cause the precision of the oscillations to deteriorate. A parallel synchrony analysis showed that the direct (between *A* and *B* and *B* and *C*) and the indirect (between *A* and *C*) couplings can be correctly identified with the use of a partial phase synchrony index; therefore, the network topology can be deduced from dynamical measurements. Numerical simulations with a locally coupled model for electrochemical chaos confirm the presence of enhanced phase fluctuations close to the transition to synchronization and the usefulness of the partial phase synchrony index for differentiation of direct from indirect interactions in a small network of oscillators.

DOI: 10.1103/PhysRevE.83.016210 PACS number(s): 05.45.Xt, 05.45.Ac, 82.40.Bj, 82.40.Np

I. INTRODUCTION

Weak interactions in small sets [1,2] and large populations [3,4] of chaotic oscillators can produce phase synchronization where the phase differences between oscillator pairs are bounded. Depending on the extent of phase coherence of the chaotic behavior three major routes to phase synchronization were observed with the Rössler system [5]. With strongly phase coherent chaotic behavior zero Lyapunov exponents are associated with the phase dynamics, and phase synchronization occurs shortly after the transition of one zero Lyapunov exponent to a negative value. The phase of a single chaotic oscillator exhibits diffusion on large time scales due to the long-term unpredictable effect of amplitudes on the phase dynamics [6–9]. This observation led to the fruitful concept of comparing features of chaotic phase synchronization to those of noisy periodic oscillations [1,3,7]. Stochastic phase models have been constructed [10–12] to describe the changes of frequencies and phase diffusion coefficients (D) of coupled chaotic oscillators as a function of coupling strength. In particular, it was shown in numerical simulations that D values obtained from both phases [8,13] and phase differences [14,15] are enlarged as the synchronization boundary is approached. Stochastic phase models based on symmetric dichotomous Markov noise [11,12] were shown to be capable of interpreting the asymmetric peak of the phase diffusion coefficient (obtained from the phase differences) as a function of coupling strengths. The analyses of phase diffusion coefficients thus imply that chaotic fluctuations are critically enhanced close to the transition to synchronization.

The phase diffusion coefficient of a chaotic oscillator is an important property that can be related to the precision of the "peak-to-peak" period of the oscillations. In biology, substantial attention is dedicated to the collective enhancement of precision in synchronous oscillating units: "noisy" oscillating cells are believed to improve their precision through synchronization [16–18]. Regularization of synchronized bursting oscillations was observed in chaotic maps [19]. With noisy periodic oscillations, factors such as the manner in which noise enters the system and coupling among oscillators are critical in determining the improved limits of precision [20].

In this paper, we investigate experimentally the phase dynamics and synchronization properties of a small network of three locally coupled (phase coherent) chaotic electrochemical oscillators. The experiments are designed to address the importance of the coupling induced changes in the precision of periods and of the effectiveness of the partial phase synchronization index [21] in differentiating direct from indirect interactions in a small network of oscillators. The electrochemical system, Ni dissolution in sulfuric acid [22] on electrode arrays [23,24], was previously utilized to characterize the transition to chaotic phase synchronization in globally coupled two- [25] and 64- [26,27] oscillator setups. Here we chose a locally coupled three-oscillator configuration representing a simple network that incorporates both directly and indirectly coupled oscillators. Experiments are performed at various local coupling strengths and the transition to phase synchronization is characterized by analysis of diffusion coefficients and bivariant and partial phase synchronization indices. Based on information from synchrony analyses, an attempt is made to differentiate direct and indirect connections in the small network. The experimental findings related to the loss of precision of chaotic oscillations close to the synchronization transition and the capability of the partial phase synchronization index to differentiate direct from indirect connections are further tested in a numerical simulation of the chemical process.

II. EXPERIMENTAL AND NUMERICAL METHODS

A. Experimental setup

A standard electrochemical cell consisting of a nickel working electrode array (Goodfellow Cambridge Ltd, 99.98%,

*izkiss@slu.edu

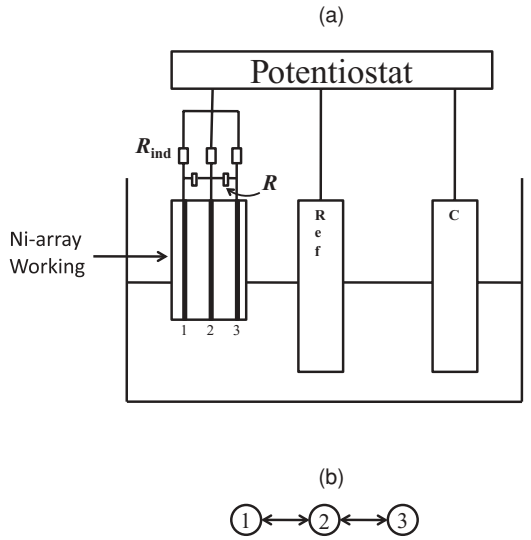

FIG. 1. Experimental setup. (a) Schematic diagram of electrochemical cell. Ref., Hg/Hg_2SO_4/sat. K_2SO_4 reference electrode; C, Pt electrode; R_{ind}, individual resistors; R, coupling resistors. (b) Coupling topology implemented by the applied resistors: three locally coupled oscillators.

1.0 mm diameter), a Hg/Hg_2SO_4/saturated K_2SO_4 reference electrode, and a platinum counterelectrode is used in the experiment [Fig. 1(a)]. The electrode array is made of three 1 mm Ni wires in linear configuration with 2 mm spacing embedded in epoxy so that reaction takes place only at the end. The electrode array is wet polished with a series of sandpapers (P180–P4000) with a Buehler Metaserv 3000 polisher. The experiments are carried out in 4.5 mol/l sulfuric acid solution at 10 °C maintained by a Neslab RTE-7 circulating bath. An external resistance $R_{ind} = 1300\ \Omega$ [see Fig. 1(a)] is added to each electrode in the array. The currents (obtained from potential drops across the external resistances) are acquired with a National Instruments (PCI 6255) data acquisition board with 200 Hz data acquisition rate. The electrode array connected to a potentiostat (ACM Instruments, Gill AC) is polarized at a constant circuit potential V. Two identical coupling resistances R (varying between 0.1 and 1000 kΩ) are introduced between the Ni electrodes in order to induce local interactions between electrodes 1, 2 and 3 as shown in Figs. 1(a) and 1(b). A typical data file consists of about 670 oscillations with 182 data points per cycle. The solution is stirred slowly with a magnetic stirrer in order to remove O_2 formed by water electrolysis.

B. Frequency and phase of oscillation

The Hilbert transform of the current $i(t)$,

$$H(t) = \frac{1}{\pi}\mathrm{PV}\int_{-\infty}^{\infty}\frac{i(\tau)-\langle i\rangle}{t-\tau}d\tau \tag{1}$$

is used in defining the phase [7,28] $\phi(t)$,

$$\phi(t) = \arctan\frac{H[i(t)]}{i(t)}. \tag{2}$$

PV in Eq. (1) implies that the integral should be evaluated in the sense of the Cauchy principal value. $\langle\,\rangle$denotes the temporal average. The frequency of an oscillator is obtained from a linear fit of $\phi(t)$ vs t,

$$\omega = \frac{1}{2\pi}\left\langle\frac{d\phi}{dt}\right\rangle. \tag{3}$$

For further analysis, the phase of the oscillations $\phi(t)$ was filtered with a first order Savitzky-Golay filter [29] with a width corresponding to the period $(1/\ \omega)$ of the oscillations. The filter removes in-cycle fluctuations that are often observed with the Hilbert-transform phase reconstruction method [30].

C. Phase diffusion coefficient

In order to evaluate the extent of phase fluctuations, the phase variance [7,13] is defined as

$$\sigma^2(\tau) = \langle[\Phi(t+\tau)-\Phi(t)]^2\rangle, \tag{4}$$

where $\Phi(t) = \phi(t) - 2\pi\omega t$ is the "detrended phase." To evaluate the variance the data file was divided into segments withτ time lengths and initial time of t_0. σ^2 is obtained as the variance of the $\Phi(t_0+\tau)-\Phi(t_0)$ values for the segments. The phase diffusion coefficient D is obtained from the slope of a linear least squares fit to the $\sigma^2(\tau)$ vs τ plot [13,14]:

$$\sigma^2(\tau) = B_1\tau + B_2 \tag{5}$$

and

$$D = B_1/2. \tag{6}$$

The error of D is evaluated from the 95% confidence interval obtained from the linear least squares fit for B_1. (The confidence interval for D was typically found to be ±1%–5%; close to the transition to synchronization we have observed errors about ±5%–10%.) The phase diffusion coefficient was also determined from the phase difference $\Delta\phi_{k,l} = \phi_k(t) - \phi_l(t)$ between any two oscillators k and l. In this case, the detrended phase is obtained by replacing the phase $\phi(t)$ with the phase difference between oscillators. The phase diffusion coefficient from the phase difference $(D_{k,l})$ is obtained from the slope of a linear least squares fit to the $\sigma^2(\tau)$ vs τ as discussed above. The phase diffusion coefficient was treated as a measure of the precision of the period of chaotic oscillations in a previous study with a single electrode [31].

D. Synchronization index

The extent of synchrony between two oscillators in the locally coupled three-oscillator setup is characterized by two indices [21] : the bivariant phase synchronization index (ρ) and the partial phase synchronization index (ρ^z). The absolute value of the bivariant phase synchronization index,

$$|\rho_{k,l}| = |\langle e^{j\Delta\phi_{k,l}(t)}\rangle|, \tag{7}$$

is a measure of the extent of phase synchronization based on the phase difference between two oscillators. (j is the imaginary unit.) The partial phase synchronization index is defined as

$$\left|\rho^z_{k,l}\right| = \frac{\left|S^{-1}_{k,l}\right|}{\sqrt{S^{-1}_{k,k}S^{-1}_{l,l}}}, \tag{8}$$

where $S^{-1}_{k,l}$ denotes the elements of the inverse of the synchronization matrix S:

$$S = \begin{pmatrix} 1 & \rho_{1,2} & \rho_{1,3} \\ \rho^*_{1,2} & 1 & \rho_{2,3} \\ \rho^*_{1,3} & \rho^*_{2,3} & 1 \end{pmatrix}. \quad (9)$$

The combined application of bivariant and partial phase synchronization measures can be utilized to infer topological features of the coupling of a small network of oscillators: numerical simulations of three locally coupled phase coherent Rössler oscillators show [21] that direct connections between oscillators k and l are indicated by large values of both $|\rho_{k,l}|$ and $|\rho^z_{k,l}|$; with indirect interactions large values of $|\rho_{k,l}|$ are accompanied by low values of $|\rho^z_{k,l}|$.

E. Model and numerical methods

To support the experimental results, numerical simulations are carried out with a prototype model of electrochemical chaos proposed by Koper and Gaspard [32]. The model has three (dimensionless) variables for each oscillator $l = 1,2,3$: the double-layer electrode potential (e_l) and the concentrations of electroactive species near the electrode surface and at the diffusion layer, u_l and w_l, respectively. The model for a three-oscillator setup coupled through cross resistances is as follows:

$$\begin{aligned} c_l \frac{de_l}{dt} &= \frac{V - e_l}{r_{\text{ind}}} - 120k(e_l)u_l + \frac{E_l}{r}, \\ \frac{du_l}{dt} &= -1.25d^{0.5}k(e_l)u_l + 2d(w_l - u_l), \\ \frac{dw_l}{dt} &= 1.6d(2 - 3w_l + u_l), \end{aligned} \quad (10)$$

where $k(e)$ is the dimensionless heterogeneous rate constant defined as

$$k(e) = 2.5\theta^2 + 0.01\exp[0.5(e - 30)] \quad (11)$$

and θ is the surface coverage of inhibiting chemical species given by a sigmoidal function

$$\theta = \begin{cases} 1 & \text{for} \quad e \leqslant 35, \\ \exp[-0.5(e - 35)^2] & \text{for} \quad e > 35. \end{cases} \quad (12)$$

Model parameters $d = 0.119\,13$, $V = 36.7395$, and $r_{\text{ind}} = 0.02$ were chosen to produce phase coherent chaotic dynamics [25,32]. As in previous studies [25], the inherent heterogeneities of the oscillators due to varying surface conditions are modeled by slightly different values of the model parameter $c_l = 1.003,0.995,0.988\,897$, for $l = 1,2,3$, respectively.

The electrical coupling among the electrodes imposed by the resistors is modeled by the coupling terms E_l in (10):

$$\begin{aligned} E_1 &= e_2 - e_1, \\ E_2 &= e_1 - 2e_2 + e_3, \\ E_3 &= e_2 - e_3. \end{aligned} \quad (13)$$

The set of ordinary differential equations was solved with MATLAB using a variable stepsize fourth-order Runge Kutta algorithm (ODE45).

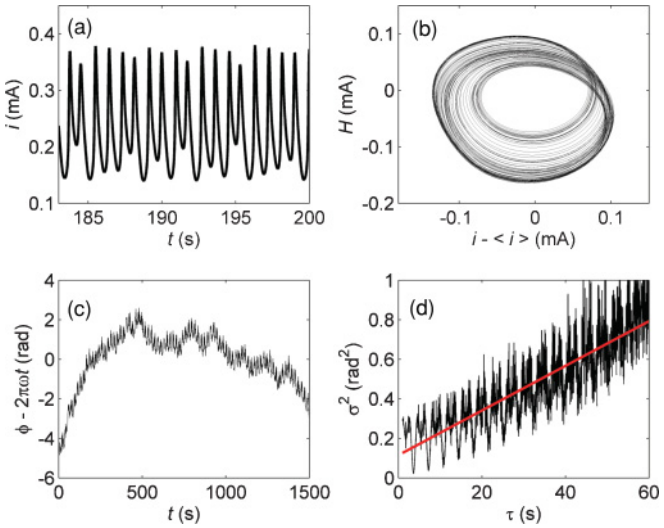

FIG. 2. (Color online) Experiments: Phase dynamics of a single phase coherent chaotic oscillator. (a) Time series of current. (b) Two-dimensional embedding using the Hilbert transform of the current. (c) Detrended phase vs time. (d) Phase variance vs time; line indicates least squares fit used to determine phase diffusion coefficient, $5.65 \times 10^{-3} \pm 0.06 \times 10^{-3}$ rad^2/s. $V = 1293$ mV.

III. RESULTS

A. Experiments

1. Single phase coherent chaotic oscillator

Dynamical features of the chaotic oscillations observed in the experiments are shown in Fig. 2. As reported in a previous study [31], the time trace of currents shown in Fig. 2(a) exhibits phase coherent character at a temperature of 10 °C. The two-dimensional phase space reconstructed using the Hilbert transform approach [Fig. 2(b)] exhibits a unique centre of rotation around the origin; therefore, the phase and frequency of the time series can be obtained. In accordance with the phase coherent character, the detrended phase of the time series shows small fluctuations in Fig. 2(c): for an experimental time of 1500 s corresponding to 1662 oscillations the largest deviation (5 rad) was less than one cycle. The diffusion coefficient obtained from the phase variance vs time plot in Fig. 2(d) was found to have the small value of $5.65 \times 10^{-3} \pm 0.06 \times 10^{-3}$ rad^2/s. We shall use this phase coherent chaotic behavior to investigate the effects of coupling in locally coupled three-oscillator configurations.

2. Three phase coherent oscillators without added coupling

The current vs time series of three chaotic oscillators without added coupling, i.e., with infinite coupling resistance R, are shown in Fig. 3(a). As in previous two- [25], three- [23], and 64- [33] oscillator experiments, we have not observed phase synchronization among the oscillators without added coupling; the phase differences between the oscillators increase linearly with time as shown in Fig. 3(b) without the presence of preferred phase differences or phase slips. The three oscillators had slightly different frequencies of $\omega_1 = 1.167$ Hz, $\omega_2 = 1.174$ Hz, and $\omega_3 = 1.191$ Hz. The phase fluctuations of the three oscillators were very small [see Fig. 3(c)] resulting in

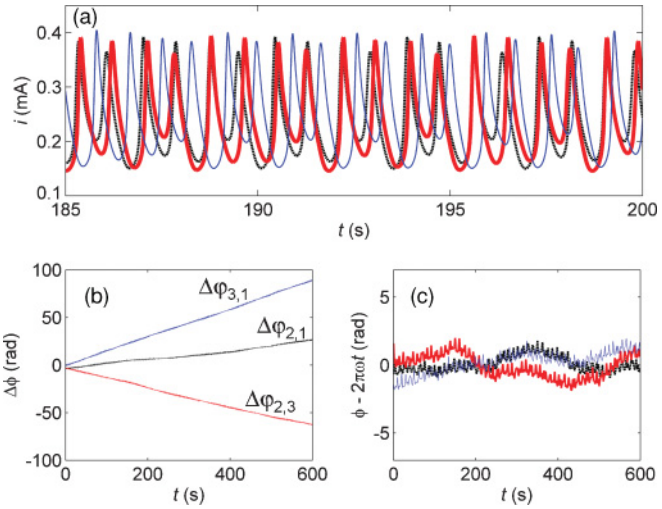

FIG. 3. (Color online) Experiments: Dynamics of three oscillators without added coupling. (a) Current time series of oscillators. (b) Phase differences ($\Delta\phi_{1,2}$, $\Delta\phi_{2,3}$, and $\Delta\phi_{1,3}$) vs time. (c) Detrended phases vs time. $V = 1300$ mV. In (a) and (c) oscillators 1, 2, and 3 are shown with dashed, thick, and thin curves, respectively.

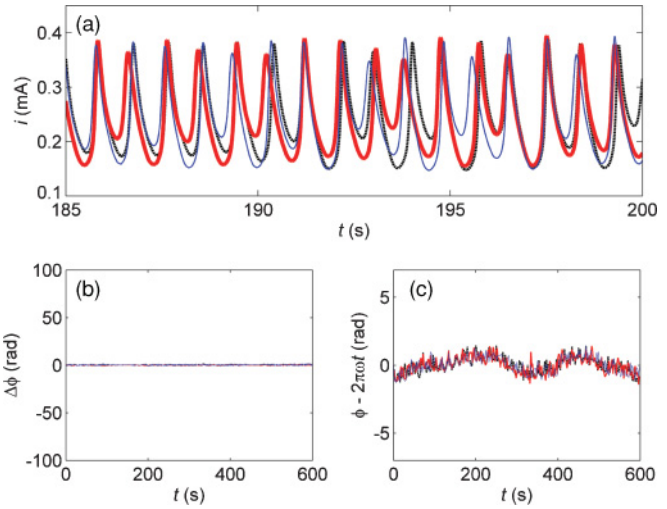

FIG. 5. (Color online) Experiments: Dynamics of three strongly coupled oscillators. (a) Current time series of oscillators. (b) Phase differences vs time. (c) Detrended phases of oscillators. $V = 1307$ mV, $R = 25$ kΩ. In (a) and (c) oscillators 1, 2, and 3 are shown with dashed, thick, and thin curves, respectively.

small values of the phase diffusion coefficients $D_1 = 5.70 \times 10^{-3} \pm 0.07 \times 10^{-3}$ rad^2/s, $D_2 = 4.49 \times 10^{-3} \pm 0.08 \times 10^{-3}$ rad^2/s, and $D_3 = 6.00 \times 10^{-3} \pm 0.09 \times 10^{-3}$ rad^2/s. The three-electrode setup without added external coupling thus represents three phase coherent chaotic oscillators with small heterogeneities in frequencies and phase diffusion coefficients.

3. *Three weakly coupled phase coherent oscillators*

The effect of weak coupling through the addition of two 150 kΩ coupling resistances between oscillators 1, 2 and 3 is shown in Fig. 4. Although the time series data of currents in Fig. 4(a) do not exhibit any obvious (e.g., identical) synchronization, the phase dynamics plots in Figs. 4(b) and 4(c) show striking differences compared to the uncoupled [Figs. 3(b) and 3(c)] results. The phase differences of the oscillators alternate periods when phase locking is observed as a plateau in $\Delta\phi$ vs t plots (such as for $200 < t < 320$ s for oscillators 1 and 2), with periods of phase drifts (such as for $320 < t < 430$ s for oscillators 1 and 2). Because of the intermittent phase locking behavior, the frequencies of the oscillators are close to each other: $\omega_1 = 1.101$ Hz, $\omega_2 = 1.113$ Hz, and $\omega_3 = 1.109$ Hz. In addition, detrended phases exhibited relatively high fluctuations [see Fig. 4(c)] compared to those of the uncoupled oscillators in Fig. 3(c). The enhanced phase fluctuations were marked by large phase diffusion coefficients $D_1 = 2.26 \times 10^{-2} \pm 0.01 \times 10^{-2}$ rad^2/s, $D_2 = 8.26 \times 10^{-2} \pm 0.05 \times 10^{-2}$ rad^2/s, and $D_3 = 9.72 \times 10^{-3} \pm 0.01 \times 10^{-3}$ rad^2/s, i.e., the values have increased by factors of 4.0, 18.4, and 1.6 for oscillators 1, 2, and 3, respectively. Thus we can see that before phase synchronization is fully established, the oscillators exhibit enlarged phase diffusion coefficients.

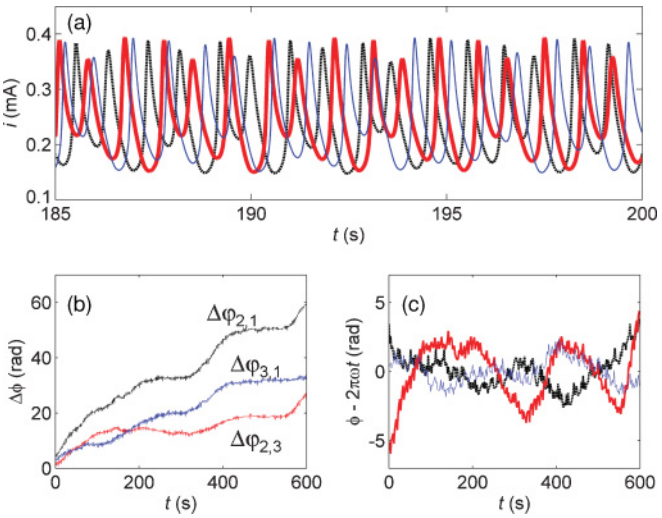

FIG. 4. (Color online) Experiments: Dynamics of three moderately coupled oscillators. (a) Current time series of oscillators. (b) Phase differences vs time. (c) Detrended phases of oscillators. $V = 1307$ mV, $R = 150$ kΩ. In (a) and (c) oscillators 1, 2, and 3 are shown with dashed, thick, and thin curves, respectively.

4. *Three strongly coupled phase coherent oscillators*

With further increase of the coupling strength, a transition to phase synchronized behavior was observed. Figure 5 shows the behavior at about six times the coupling strength (with coupling resistance of 25 kΩ) as that in Fig. 4. Although identical synchronization is still not observed in the current vs time series data in Fig. 5(a), it is clearly seen that the oscillators "spike" at about the same time (with small jitter) for every oscillation. At this coupling strength the frequencies of all the oscillators were found to be 1.110 Hz and the phase difference between any two oscillators was close to a constant value (zero) [Fig. 5(b)]. The detrended phase of oscillators shown in Fig. 5(c) exhibited small fluctuations similar to those observed with the uncoupled oscillators. Note that the detrended phases exhibit almost identical long-range trends; therefore the diffusion coefficients were found to be

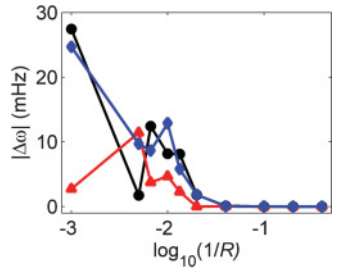

FIG. 6. (Color online) Experiments: Pairwise frequency differences vs coupling strength $\{\log_{10}[1/R\ (\mathrm{k}\Omega)]\}$. Circles, $\Delta\omega_{1,2}$; triangles, $\Delta\omega_{2,3}$; diamonds, $\Delta\omega_{1,3}$.

$D_1 = 3.09 \times 10^{-3} \pm 0.08 \times 10^{-3}$ rad^2/s, $D_2 = 2.90 \times 10^{-3} \pm 0.08 \times 10^{-3}$ rad^2/s, and $D_3 = 3.40 \times 10^{-3} \pm 0.07 \times 10^{-3}$ rad^2/s, i.e., oscillators 1, 2, and 3 exhibited 46%, 35%, and 43% decrease compared to the values obtained with uncoupled oscillators, respectively. These results indicate that the strong enhancement of phase diffusion observed before the onset of phase synchronization cannot be observed after strong phase synchronization has been established.

5. *Effect of coupling strength: Frequency difference and phase diffusion coefficient*

In order to further characterize the effect of local interactions on the dynamical features of the three-oscillator setup, we carried out a series of experiments with ten coupling strengths utilizing coupling resistances in the range of 2.5 to 1000 kΩ. The frequency differences for each of the three pairs of oscillators as a function of coupling strength ($1/R$ on a logarithmic scale) are shown in Fig. 6. With increase of coupling, there is a strong tendency for the frequency differences to decrease; however, the transitions are not monotonic as would be expected for a pair of oscillators with symmetrical coupling [34]. The nonmonotonic variations are probably affected by the inherent drift of the oscillator frequencies which are on the order of 0–5 mHz/experiment; however, as will be shown in the numerical simulation section, coupling can increase the frequency difference between oscillators due to effects similar to anomalous phase synchronization [35]. Oscillators 2 and 3 become synchronized at $R = 50$ kΩ, after which full synchrony is achieved with $R = 25$ kΩ$[\log_{10}(1/R) = -1.40]$. With an increase of the coupling strength above these threshold values, the frequency differences remained zero.

The variation of the phase diffusion coefficients with coupling strength for oscillators 1, 2, and 3 is shown in Figs. 7(a), 7(b), and 7(c), respectively. The common feature of the curves is the strongly enlarged phase diffusion coefficient before the onset of phase synchronization. Oscillators 1 and 2 exhibit an approximately single-peak variation with a maximum at $R = 75$ and 150 kΩ, respectively; oscillator 3 exhibits an approximate double-peak behavior with local maxima at $R = 75$ and 200 kΩ. All these peaks occur close to but

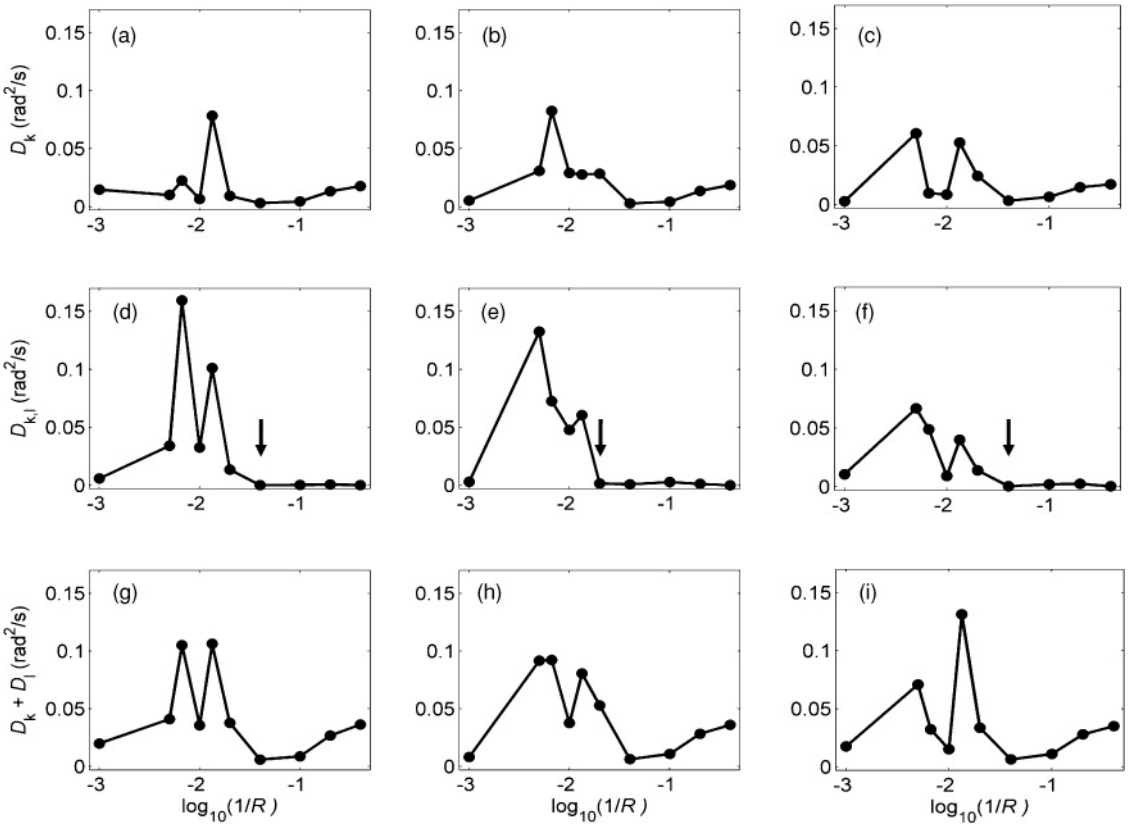

FIG. 7. Experiments: Measures of phase fluctuations as functions of the coupling strength. Top: Phase diffusion coefficient vs coupling strength, (a) D_1, (b) D_2, (c) D_3. Middle: Phase diffusion coefficient determined from phase difference between oscillators vs coupling strength, (d) $D_{1,2}$, (e) $D_{2,3}$, (f) $D_{1,3}$. Bottom: Sum of phase diffusion coefficients vs coupling strength, (g) $D_1 + D_2$, (h) $D_2 + D_3$, (i) $D_1 + D_3$. Arrows indicate onset of phase synchronization.

distinctly before the transition to phase synchronization ($R =$ 25–50 kΩ). These peaks represent a dramatic enlargement of D at the global maxima; for oscillators 1, 2, and 3, the D values increase by factors of 14, 18, and 10, repectively, compared to the values of the uncoupled oscillators. After the maximum (for oscillator 3 the second maximum) the D values decrease. In this region, with a pair of Rössler oscillators it was found that $D_{1,2}/(2\pi\,\Delta\omega_{1,2}) \approx \pi$ [11]. For the experimental data with three oscillators, close to the synchronization transitions where the frequency differences were smaller than 6 mHz, the $D_{k,l}/(2\pi\,\Delta\omega_{k,l})$ values were found to be within a range of 0.3π–1.5π. We thus see that for the three-oscillator setup the order of magnitude of the phase diffusion coefficient is consistent with the theoretical prediction [11]. Immediately after the transition to phase synchronization, the phase diffusion coefficients take up values similar to those seen with the uncoupled oscillators.

The dependencies of the phase diffusion coefficients determined from the phase differences between two oscillators ($D_{1,2}$, $D_{2,3}$, and $D_{1,3}$) on the coupling strength are shown in Figs. 7(d)–7(f). Before the phase synchronization transition, the oscillators are weakly correlated and therefore the variations are expected to follow the sum of the phase diffusion coefficients of the individual oscillators ($D_{k,l} \approx D_k + D_l$). For convenience, the $D_k + D_l$ quantities are plotted in Figs. 7(g)–7(i). Before the transition to synchronization, the values of $D_k + D_l$ are good indicators of $D_{k,l}$: for oscillators 1–2 [Fig. 7(d)] and 1–3 Fig.7(f)] a double-peak structure, while for oscillators 2–3 [Fig. 7(e)] a wide single-peak structure, were observed. Just before the onset of phase synchronization the $D_{k,l}$ values become diminished due to the appearance of strong correlations; after phase synchronization sets in $D_{k,l} = 0$.

The analysis of the phase diffusion coefficients based on the individual phases of oscillators and on the phase differences between oscillators thus indicates that there is great deterioration in the precision of the period of chaotic oscillators before the onset of synchronization.

6. Distinguishing direct interactions from indirect interactions

The effect of local coupling strength on the extent of synchronization was characterized with an analysis of the bivariant (7)] and partial [(8)] synchronization indices. The bivariant phase synchronization index as a function of the coupling strength is shown in Figs. 8(a)–8(c) for the oscillator pairs. The synchronization index varies between 0 (lack of synchrony) and 1 (full synchrony). For simplicity we consider it an increased level of synchrony between the oscillators if the index reaches above 0.5 (dashed line in the figures). (A more sophisticated analysis based on a twin surrogate significance level analysis [36] and recurrence based synchrony measures [37] also indicated [38] that the 0.5 value is a good cutoff level for this specific experimental system.)

For the directly coupled oscillator pairs 1–2 and 2–3, below a coupling strength corresponding to $R = 75$ and 150 kΩ, respectively, the bivariant synchrony index is smaller than 0.5, indicating lack of synchrony [see Figs. 8(a) and 8(b)]. Above the given coupling strengths, $|\rho|$ rises above 0.5 and increases monotonically as the coupling strength is increased. As in the results of the frequency analysis, the bivariant synchrony measures indicate that directly coupled oscillators 2 and 3 synchronize at weaker coupling strength than oscillators 1 and 2. At coupling strengths $R < 50$ kΩ, where both directly coupled oscillators are synchronized, the bivariant synchronization index for the indirectly coupled oscillator pair 1–3 also indicates synchronized behavior [see Fig. 8(c)]. By comparison of the variations of $|\rho|$ with the coupling strength of the directly coupled [Figs. 8(a) and 8(b)] and the indirectly coupled oscillators [Fig. 8(c)], it can be seen that the trends and values are very similar; the indirectly coupled oscillators typically have only slightly smaller values of $|\rho|$. Based on these small differences, the distinction between directly and indirectly coupled oscillators would be very difficult.

The partial phase synchronization index for the directly coupled oscillators is shown in Figs. 8(d) and 8(e). Below the transition to phase synchronization (for coupling strengths at

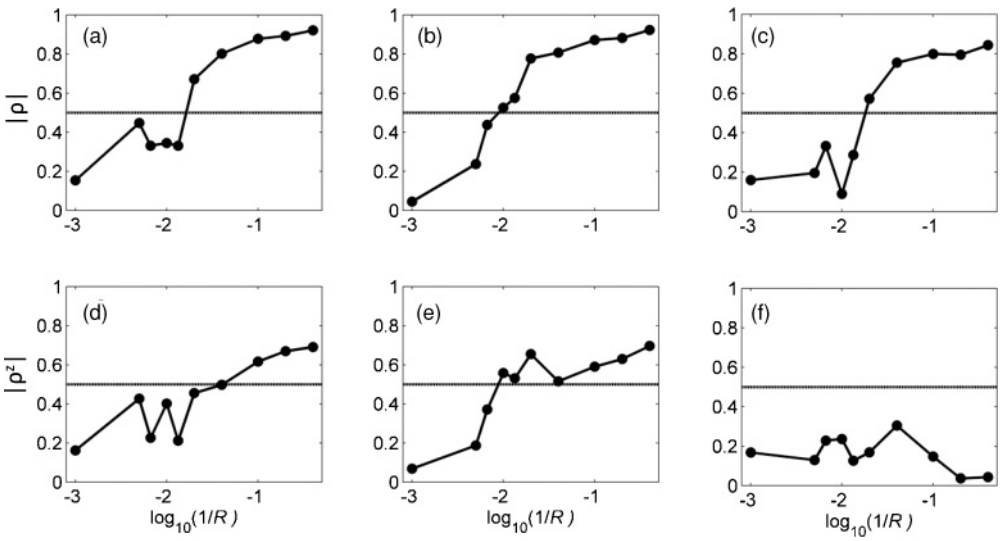

FIG. 8. Experiments: Pairwise synchronization indices vs coupling strength. Top: Bivariant synchronization index ($|\rho|$) vs coupling strength, (a) $|\rho_{1,2}|$, (b) $|\rho_{2,3}|$, (c) $|\rho_{1,3}|$. Bottom: Partial phase synchronization index ($|\rho^z|$) vs coupling strength, (e) $|\rho^z_{1,2}|$, (f) $|\rho^z_{2,3}|$, (g) $|\rho^z_{1,3}|$.

which $|\rho| < 0.5$), the partial phase synchrony index is smaller than the cutoff level ($|\rho^z| < 0.5$) and the values are similar to the corresponding values of $|\rho|$. Above the transition to phase synchronization, $|\rho^z|$ has an increasing trend with increase of the coupling strength; however, the typical values of $|\rho^z|$ are smaller than $|\rho|$ by 0.1–0.2. Nonetheless, for coupling strengths where strong phase synchrony is indicated for the directly coupled oscillators [$|\rho| > 0.8$ in Figs. 8(a) and 8(b)], the partial phase synchrony index is above the 0.5 cutoff value.

The dependence of the partial phase synchronization index on coupling strength for the indirectly coupled oscillator pair 1–3 is shown in Fig. 8(f). $|\rho^z|$ remains a small value (<0.5) for all coupling strengths; in fact it has a decreasing trend with increase of the coupling strength for strong coupling ($R < 50\text{k}\Omega$) where the corresponding bivariant phase synchronization index has an increasing trend [Fig. 8(c)] with values >0.5.

These results confirm the proposition [21] that the partial phase synchronization index characterizes the synchrony induced by direct coupling. For the directly coupled oscillator pairs 1–2 and 2–3, the partial and bivariant phase synchronization indices have similar trends and similar values. In contrast, for the indirectly coupled oscillator pair 1–3, the bivariant phase synchronization index characterizes the existing high level of synchrony due to indirect coupling through oscillator 2, but the partial phase synchronization index correctly indicates the lack of synchrony induced by direct coupling.

B. Numerical simulations

We carried out numerical simulations with a prototype electrochemical model [Eqs. (10)–(13)] to confirm the experimental findings and shed light on the details of the synchronization transition.

The dynamical features of a single phase coherent oscillator obtained by integrating Eqs. (10)–(13) for $l = 1$ and with $c_1 = 1$ are shown in Fig. 9. The chaotic oscillations with the chosen set of parameters are obtained through a periodic-doubling bifurcation with increasing parameter V [25,32]; chaotic time series data of the variable e are shown in Fig. 9(a). A two-dimensional embedding using a Hilbert transform [see Fig. 9(b)] produces a unique center of rotation as the origin. The phase was successfully obtained using the Hilbert transform approach. The frequency of the oscillations was found to be 0.475. The detrended phase exhibited extremely small fluctuations in the chosen parameter region [Fig. 9(c)]. The phase diffusion coefficient, obtained from the phase variance plot in Fig. 9(d), was found to have a very small value of $4.0 \times 10^{-5} \pm 0.2 \times 10^{-5}$. (Note that the actual values of the frequency and phase diffusion coefficients cannot be directly compared to the experimental data because the numerical model is a dimensionless, prototype model that simulates general dynamical and some limited chemical characteristics of electrochemical oscillations.)

A series of simulations were carried out for a set of coupling resistances r for the three-oscillator setup using Eqs. (10)–(13) with $l = 1,2,3$ and $c_l = 1.003$, $c_2 = 0.995$, and $c_3 = 0.988\,897$. These conditions result in a state which is similar to that observed in the experiments: phase coherent chaotic oscillations with slightly different (~1%–2%), monotonically

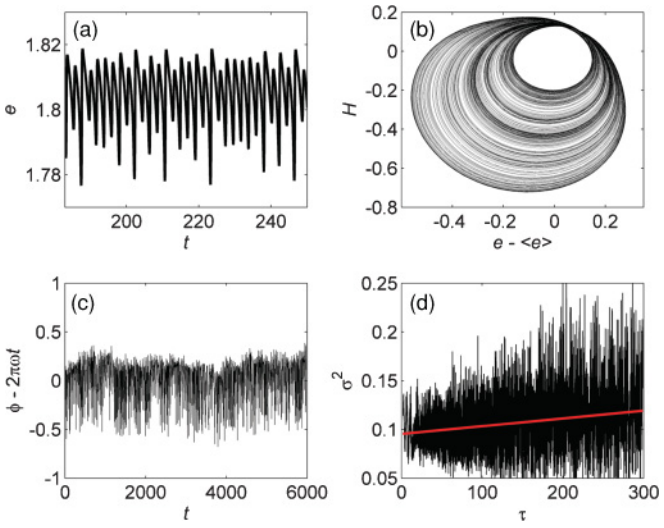

FIG. 9. (Color online) Numerical simulations: (a) Time series of variable e (electrode potential). (b) Two-dimensional embedding using Hilbert transform. (c) Detrended phase vs time. (d) Phase variance vs time; line indicates least squares fit used to determine phase diffusion coefficient $D = 4.0 \times 10^{-5} \pm 0.2 \times 10^{-5}$.

distributed frequencies. For uncoupled oscillators ($r = \infty$) the frequencies are (0.4761, 0.4733, 0.4712) with $D_1 = 2.6 \times 10^{-6} \pm 0.3 \times 10^{-6}$, $D_2 = 4.39 \times 10^{-5} \pm 0.05 \times 10^{-5}$, and $D_3 = 3.36 \times 10^{-5} \pm 0.05 \times 10^{-5}$. The frequency differences between the oscillator pairs as a function of the coupling strength are shown in Fig. 10. The frequency difference between oscillators 1 and 2 has a decreasing trend with a smoothed out transition point characteristic for a pair of coupled phase coherent oscillators [14]. Phase synchronization sets in for oscillator pair 1–2 at $r = 284$ where the frequencies become identical. While the center oscillator 2 is being synchronized to oscillator 1 with increase of coupling strength, the frequency difference between oscillators 2 and 3 increases. After synchronization of oscillator pair 1–2, the $\Delta\omega_{2,3}$ values decrease with increasing coupling strength and full phase synchronization sets in at $r = 160$. The frequency difference between the two "edge" oscillators 1 and 3 with increasing coupling strength first slightly increases up to the establishment of synchrony between oscillators 1 and 2; thereafter, it quickly decreases. The results show that, as in the experimental results, synchronization is a two-step process: the

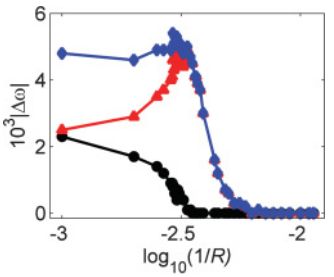

FIG. 10. (Color online) Numerical simulations: Pairwise frequency differences vs coupling strength. Circles, $\Delta\omega_{1,2}$; triangles, $\Delta\omega_{2,3}$; diamonds, $\Delta\omega_{1,3}$.

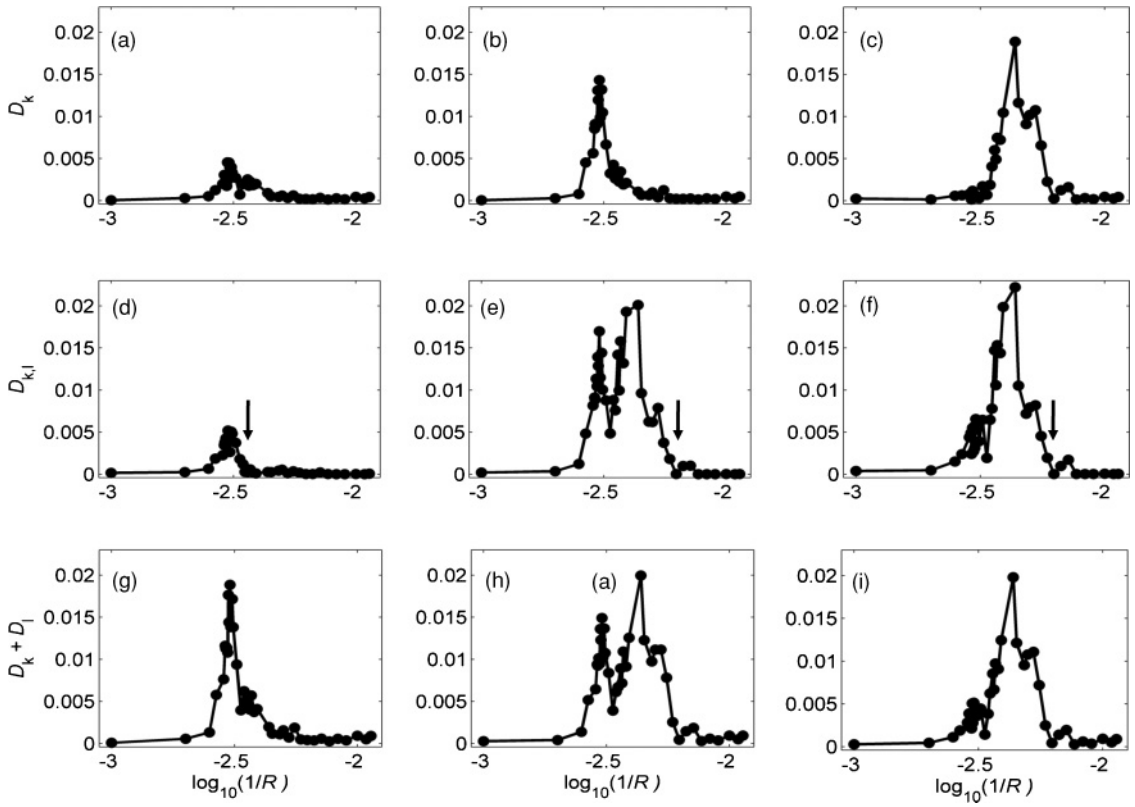

FIG. 11. Numerical simulations: Measures of phase fluctuations as a function of coupling strength. Top: Phase diffusion coefficient vs coupling strength, (a) D_1, (b) D_2, (c) D_3. Middle: Phase diffusion coefficient determined from phase difference between oscillators vs coupling strength, (d) $D_{1,2}$, (e) $D_{2,3}$, (f) $D_{1,3}$. Bottom: Sum of phase diffusion coefficients vs coupling strength, (g) $D_1 + D_2$, (h) $D_2 + D_3$, (i) $D_1 + D_3$. Arrows indicate onset of phase synchronization.

directly coupled 1–2 and 2–3 oscillators become synchronized at $r = 284$ and 160, respectively.

1. *Enhanced phase fluctuation before the onset of synchronization*

The effect of local coupling strength on the phase diffusion coefficient of the oscillators is shown in Figs. 11(a)–11(c). As in the experimental results, strongly enlarged D values were obtained at coupling strengths somewhat weaker than those required for full phase synchronization. All oscillators exhibit one major peak in the D vs coupling strength plots; however, the monotonic increase or decrease is often interrupted by small local peaks or shoulders that often coincide with the synchronization transition for a pair of oscillators (indicated by arrows). The maximum phase diffusion coefficients represent 1737-, 327-, and 562-fold enhancements over those observed with the uncoupled oscillators 1, 2, and 3, respectively. At coupling strengths with values close to phase synchronization where the frequency differences were smaller than 0.3, the $D_{k,l}/(2\pi\,\Delta\omega_{k,l})$ values were found to be within a range of 0.5π–0.9π. At coupling strengths above full phase synchronization ($r < 160$), the D values are relatively low (at least ten times lower than the maximum values).

The phase diffusion coefficients obtained from phase differences are shown Figs. 11(d)–11(f). The single-peak [oscillators 1–2, Fig. 11(d) , and 1–3, Fig. 11(f)] and double-peak [oscillators 2–3, Fig. 11(e)] trends in the figures at coupling strengths weaker than for the corresponding onset of synchronization can be explained by the behavior of the sum of the individual phase diffusion coefficients shown in Figs. 11(g) and 11(h). Above the synchronization transition the $D_{k,l}$ values go to zero as expected for phase synchronization [7].

2. *Distinguishing direct and indirect interactions*

The effect of the coupling strength on synchrony features is shown in Fig. 12. The bivariant phase synchronization index [Figs. 12(a)–12(c)] has low values for weak, and strongly elevated ($|\rho| > 0.5$) values for strong coupling. For oscillator pairs 1–2, 2–3, and 1,3 the critical resistances at which $|\rho|$ passes 0.5 are 310, 207, and 207, respectively. For directly coupled pairs [1–2, Fig. 12(a), and 2–3, Fig. 12(b)] $|\rho|$ seems to saturate at around a value of 0.7–0.8 for the coupling strength, stronger than the critical value; for the indirectly coupled pair [1–3, Fig. 12(c)] the saturation occurs at a somewhat lower value of $|\rho| \approx 0.6$.

The variation of the partial phase synchronization index with coupling strength is shown in Figs. 12(d)–12(f). For the directly coupled oscillator pairs [Figs. 12(d) and 12(e)] $|\rho^z|$ follows the same trend as $|\rho|$ [Figs. 12(a) and 12(b)] with $|\rho^z|$ having a value of 0.1–0.2 lower than $|\rho|$ for the strong coupling strengths. In contrast, for the indirectly coupled oscillator pairs [1–3, Fig. 12(f)] the partial phase synchronization index remains low for every coupling strength ($|\rho^z| < 0.4$). The results thus confirm that with strongly phase synchronized oscillators

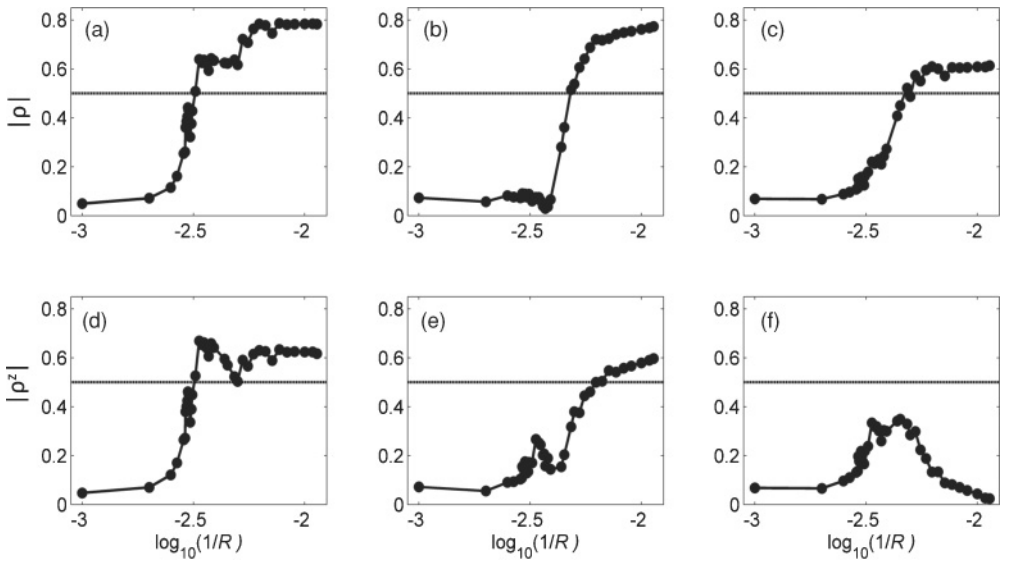

FIG. 12. Numerical simulations: Pairwise synchronization indices vs coupling strength. Top: Bivariant synchronization index ($|\rho|$) vs coupling strength, (a) $|\rho_{1,2}|$, (b) $|\rho_{2,3}|$, (c) $|\rho_{1,3}|$. Bottom: Partial phase synchronization index ($|\rho^z|$) vs coupling strength, (e) $|\rho^z_{1,2}|$, (f) $|\rho^z_{2,3}|$, (g) $|\rho^z_{1,3}|$.

($r < 160$), the directly coupled oscillator pairs (1–2 and 2–3) exhibit large (>0.5) values of both $|\rho^z|$ and $|\rho|$; oscillator pairs (1–3) exhibit large values of $|\rho|$ along with small values $|\rho^z|$, correctly indicating the lack of direct connections.

IV. DISCUSSION

Coupling through cross resistors was found to induce phase synchronization in three locally coupled chaotic phase coherent oscillators in Ni electrodissolution. The transition to synchronization took place in two steps during which with increase of coupling strength the center oscillator first synchronized to one of the edge oscillators; with further increase of coupling strength the remaining edge oscillator joined the synchronized group above a critical coupling strength.

The bivariant synchronization index [21] successfully characterized the synchronization transition by showing elevated values for each oscillator pair with coupling strengths above that for the transition to full synchronization. This result implies that, based on the bivariant phase synchronization index, it is very difficult to differentiate direct from indirect coupling in a small network. In contrast, the partial phase synchronization index [21] indicated direct corrections by elevated values for the coupling of the edge oscillators to the center oscillator. The small value of the partial phase synchronization index for the two edge oscillators indicated the lack of direct coupling. The presented results therefore provide experimental evidence that the partial phase synchronization index proposed by Schelter *et al.* [21] is a useful tool for the identification of missing coupling links in a locally coupled three-oscillator setup. The method of the partial phase synchronization index requires a definition of phase for the chaotic oscillator. For strongly non-phase-coherent chaotic oscillators, a recurrence based analysis [38] or methods based on directionality analysis [39] and permutation entropy [40] can be applied. Because in the given experimental system the extent of phase coherence can be controlled by changes in temperature [31], the experimental applicability of these methods could be tested as well.

Analysis of the variation of the phase diffusion coefficient in electrochemical experiments and numerical simulations confirmed the prediction that the precision of chaotic oscillators strongly deteriorates before the onset of synchronization. Close to (but before) the transition to synchronization at least a 10- 18-fold enhancement of phase diffusion was observed. The order of magnitude of this enhancement was in good agreement with the theoretically predicted relationship $D_{1,2}/(2\pi\Delta\omega_{1,2}) \approx \pi$ for a pair of oscillators [12]. In addition, we observed that D values obtained from both the individual phases and phase differences are enlarged. With weak coupling strengths, where the correlation between the oscillators is weak, the phase diffusion values from phase differences ($D_{k,l}$) can be approximated by the sum of the phase differences ($D_k + D_l$). This relationship could be a valuable tool in characterization of a "significant" level of coupling induced synchrony among oscillators in addition to the presently used twin surrogate [36] methodology.

We also observed that the enhancement of the phase diffusion exhibited multipeak behavior with increase of the coupling strength. When one pair of oscillators approached phase synchronization and thus exhibited enlarged phase diffusion, the remaining, weakly coupled oscillator might also exhibit at least some enhancement of phase diffusion. The multipeak behavior in curves of D vs coupling strength has been observed in numerical simulations with three globally coupled Rössler oscillators [15]; therefore it seems that the theory of two coupled oscillators [11,12,14,15], at least qualitatively, is applicable to the three-oscillator configuration.

The experiments in this study were carried out with electrochemical oscillations; however, the studied underlying phenomena related to synchrony features of directly and indirectly coupled oscillations and the precision of the period of oscillations have important roles in many biological examples

such as the precision and coupling of circadian oscillators [41]. We note that the oscillators in this study are nonprecise because of some inherent dynamical causes that result in chaotic behavior. The deterioration of precision is related to the appearance of complicated correlated amplitude (noise) effects. This scenario could be important in the functioning of dynamical clocks that are strongly intertwined but exhibit very different time scales so that that a "stochastic" approach could be applied to simplify the long-term effect of chaotic variations.

ACKNOWLEDGMENTS

Acknowledgments are made to the Research Corporation for Science Advancement and the President's Research Fund of Saint Louis University for support of this research.

[1] M. G. Rosenblum, A. S. Pikovsky, and J. Kurths, Phys. Rev. Lett. **76**, 1804 (1996).
[2] K. J. Lee, Y. Kwak, and T. K. Lim, Phys. Rev. Lett. **81**, 321 (1998).
[3] A. S. Pikovsky, M. G. Rosenblum, and J. Kurths, Europhys. Lett. **34**, 165 (1996).
[4] E. Ott *et al.*, Physica D **173**, 29 (2002).
[5] G. V. Osipov, B. Hu, C. Zhou, M. V. Ivanchenko, and J. Kurths, Phys. Rev. Lett. **91**, 024101 (2003).
[6] J. D. Farmer, Phys. Rev. Lett. **47**, 179 (1981).
[7] A. S. Pikovsky, M. G. Rosenblum, and J. Kurths, *Synchronization—A Universal Concept in Nonlinear Sciences* (Cambridge University Press, Cambridge, England, 2001).
[8] E. Rosa, E. Ott, and M. H. Hess, Phys. Rev. Lett. **80**, 1642 (1998).
[9] V. S. Anishchenko, T. E. Vadivasova, J. Kurths, G. A. Okrokvertskhov, and G. I. Strelkova, Phys. Rev. E **69**, 036215 (2004).
[10] W. H. Kye, D. S. Lee, S. Rim, C. M. Kim, and Y. J. Park, Phys. Rev. E **68**, 025201 (2003).
[11] T. Yamada *et al.*, Prog. Theor. Phys. **116**, 819 (2006).
[12] T. Horita *et al.*, Prog. Theor. Phys. **119**, 223 (2008).
[13] A. S. Zakharova, T. E. Vadivasova, and V. S. Anishchenko, Int. J. Bifurcation Chaos Appl. Sci. Eng. **18**, 2877 (2008).
[14] H. Fujisaka *et al.*, Physica D **205**, 41 (2005).
[15] T. Kono *et al.*, Prog. Theor. Phys. Suppl. **161**, 240 (2006).
[16] A. T. Winfree, *The Geometry of Biological Time* (Springer-Verlag, New York, 1980).
[17] J. Garcia-Ojalvo, M. B. Elowitz, and S. H. Strogatz, Proc. Natl. Acad. Sci. USA **101**, 10955 (2004).
[18] E. D. Herzog *et al.*, J. Biol. Rhythms **19**, 35 (2004).
[19] N. F. Rulkov, Phys. Rev. Lett. **86**, 183 (2001).
[20] D. J. Needleman, P. H. E. Tiesinga, and T. J. Sejnowski, Physica D **155**, 324 (2001).
[21] B. Schelter, M. Winterhalder, R. Dahlhaus, J. Kurths, and J. Timmer, Phys. Rev. Lett. **96**, 208103 (2006).
[22] O. Lev *et al.*, J. Phys. Chem. **93**, 1661 (1989).
[23] I. Z. Kiss, W. Wang, and J. L. Hudson, J. Phys. Chem. B **103**, 11433 (1999).
[24] I. Z. Kiss, V. Gáspár, and J. L. Hudson, J. Phys. Chem. B **104**, 7554 (2000).
[25] I. Z. Kiss and J. L. Hudson, Phys. Chem. Chem. Phys. **4**, 2638 (2002).
[26] I. Z. Kiss, Y. Zhai, and J. L. Hudson, Phys. Rev. Lett. **88**, 238301 (2002).
[27] I. Z. Kiss, Y. M. Zhai, and J. L. Hudson, Science **296**, 1676 (2002).
[28] A. S. Pikovsky *et al.*, Physica D **104**, 219 (1997).
[29] W. H. Press, S. A. Teukolsky, W. T. Vetterling, and B. P. Flannery, *Numerical Recipes: The Art of Scientific Computing*, 3rd ed. (Cambridge University Press, New York, 2007).
[30] B. Kralemann, L. Cimponeriu, M. Rosenblum, A. Pikovsky, and R. Mrowka, Phys. Rev. E **77**, 066205 (2008).
[31] M. Wickramasinghe and I. Z. Kiss, Chaos **20**, 023125 (2010).
[32] M. T. M. Koper and P. Gaspard, J. Chem. Phys. **96**, 7797 (1992).
[33] I. Z. Kiss, Y. M. Zhai, and J. L. Hudson, Phys. Rev. Lett. **94**, 248301 (2005).
[34] S. H. Strogatz, *Nonlinear Dynamics and Chaos* (Westview Press, Cambridge, MA, 2000).
[35] B. Blasius, E. Montbrio, and J. Kurths, Phys. Rev. E **67**, 035204 (2003).
[36] M. Thiel *et al.*, Europhys. Lett. **75**, 535 (2007).
[37] M. C. Romano *et al.*, Europhys. Lett. **71**, 466 (2005).
[38] J. Nawrath, M. C. Romano, M. Thiel, I. Z. Kiss, M. Wickramasinghe, J. Timmer, J. Kurths, and B. Schelter, Phys. Rev. Lett. **104**, 038701 (2010).
[39] B. Kralemann, L. Cimponeriu, M. Rosenblum, A. Pikovsky, and R. Mrowka, Phys. Rev. E **76**, 055201 (2007).
[40] A. Bahraminasab, F. Ghasemi, A. Stefanovska, P. V. E. McClintock, and H. Kantz, Phys. Rev. Lett. **100**, 084101 (2008).
[41] E. D. Herzog, Nat. Rev. Neurosci. **8**, 790 (2007).